Journal of Luminescence 183 (2017) 113–120

Contents lists available at ScienceDirect

Journal of Luminescence

journal homepage: www.elsevier.com/locate/jlumin

Influence of 3D aggregation on the photoluminescence dynamics of CdSe quantum dot films

T. Alejo [a], Pedro M.R. Paulo [b], M.D. Merchán [a], Emilio Garcia-Fernandez [b,1], Sílvia M.B. Costa [b], M.M. Velázquez [a,*]

[a] Departamento de Química Física, Facultad de Ciencias Químicas, Universidad de Salamanca, E-37008 Salamanca, Spain
[b] Centro de Química Estrutural, Instituto Superior Técnico, Universidade Técnica de Lisboa, Av. Rovisco Pais 1, 1049-001 Lisboa, Portugal

ARTICLE INFO

Article history:
Received 5 July 2016
Received in revised form
3 November 2016
Accepted 4 November 2016
Available online 9 November 2016

Keywords:
Quantum dots
Langmuir-blodgett films
Confocal fluorescence lifetime microscopy
Photoluminescence properties

ABSTRACT

Thin films of semiconductor CdSe quantum dots, QDs, directly deposited onto quartz as well as onto a Langmuir-Blodgett film of the Gemini surfactant ethyl-bis (dimethyl octadecyl ammonium bromide have been prepared and their photoluminescence properties were characterized by confocal fluorescence lifetime microscopy. 3D aggregates of QDs were observed in QD films directly deposited onto the solid while the Gemini surfactant film avoids the 3D aggregation. The photoluminescence decay analysis was performed by a phenomenological model previously proposed by us which considers that the luminescence dynamics is affected by energy transport and trapping processes and the relative contribution of these processes depends on film morphology. Thus, in the non-aggregated and more homogeneous QD films, QDs deposited onto the surfactant, the relative contribution of the energy transport process increases with trap concentration while 3D aggregation favors the energy transport even at low density of energy traps.

1. Introduction

Semiconductor nanocrystals have a huge potential for application in biological research, photonic studies, and optoelectronic devices [1–4]. One of its most important classes is colloidal nanocrystals, such as CdTe and CdSe. Due to quantum confinement, these nanocrystals possess discrete electron and hole energy levels [5,6] and as a consequence, optical absorption occurs at discrete energies which are determined by the size and the shape of nanocrystals [2]. At low excitation density, light emission is due to decay of the lowest exciton state to the ground state. The possibility of tuning the exciton emission energy by the nanocrystal size or shape has led to a worldwide interest in light-emitting semiconductor nanocrystals. It is well established that the optoelectronic properties of quantum dots depend on the surface defects. [7] Moreover, in devices employing QDs deposited onto solids, surface defects play a dominant role in the photoluminescence properties. In this situation, the surface defects depend not only on the value of the surface area but also on the morphology of QD assemblies. In previous work we have analyzed the photoluminescence of CdSe QDs and styrene maleic anhydride polymer films prepared by the Langmuir-Blodgett methodology [8]. We have chosen the Langmuir-Blodgett deposition methodology because it has provided good quality nanoparticle thin films [9–11] and offers the possibility of preparing reproducible films with control of the interparticle distance. Our results demonstrated that the photoluminescence dynamics are strongly affected by excitation energy transport and trapping processes and the efficiency of each process depends on the interdot distance and on the surface density of traps, which were related with QD clustering or surface defects. The results also pointed out that the photoluminescence of QDs should be increased by a homogeneous distribution of QDs in films and by minimizing the surface defects [8]. To confirm these assumptions, in the current work we compare the photoluminescence properties of homogeneously distributed QDs films with heterogeneous films of QDs directly deposited onto the solid substrate. To prepare homogeneous films, we transferred QDs from the air-water interface to a Langmuir-Blodgett film of the Gemini surfactant ethyl-bis (dimethyl octadecylammonium bromide). We use this deposition methodology since the surfactant film avoids the 3D aggregation of QDs which is obtained when nanocrystals are directly deposited onto the substrate [12–16]. In addition, the surfactant renders an almost continuous film of QDs distributed in an ideal hexagonal array [14].

* Corresponding autor.
E-mail address: mvsal@usal.es (M.M. Velázquez).
[1] Present address: Department of Physical Chemistry, Faculty of Pharmacy, University of Granada, Campus Cartuja, 18071 Granada, Spain

http://dx.doi.org/10.1016/j.jlumin.2016.11.002
0022-2313/

2. Experimental

2.1. Materials and methods

CdSe QDs capped with trioctylphosphine oxide (TOPO) were synthesized by the method reported by Yu and Peng [17] and described in more detail by Tomczak [18]. QDs were collected as power by precipitation and centrifugation with acetone. Centrifugation with acetone was used to wash the QDs in order to remove free capping ligands and other molecules of the synthesis medium. The process was repeated at least three times to remove all free ligand and molecules. All these molecules were separated of QDs power because they can be dissolved in acetone. The QDs thus obtained were dried under vacuum and the diameter (3.55 ± 0.05 nm) was calculated from the maximum position of the visible spectrum of QDs dispersed in chloroform and the extinction coefficient per mole of nanocrystals at the first excitonic absorption peak [19]. UV–vis absorption spectra of nanocrystal solutions were recorded on a Shimadzu UV-2401PC spectrometer. The stabilizer ligand (TOPO) remains attached to the QD surface after the purification and precipitation processes [20–22].

Gemini surfactant ethyl-bis(dimethyl octadecylammonium bromide), ($M_r = 783.02$) was synthesized using the method described by Zana et al. [23]. We introduced some modifications in the purification procedure to improve the product purity [12]. The degree of purity obtained by mass spectrometry was $> 99.9\%$.

Filtered Chloroform (PAI) was supplied from Sigma Aldrich and ultra pure water used as subphase to build the Langmuir monolayers were obtained by combination of RiOs and MilliQ systems from Millipore. The solid substrate Quartz was supplied by Ted Pella (US) and prior deposition was cleaned by the RCA process [24] to remove organic residues from quartz substrates [25]. Briefly, the substrate was successively cleaned with acetone (PAI), ethanol (PAI) and water (Milli Q); then, it was submerged in 60 mL of a cleaning solution of MilliQ water, ammonia (25%) (5:1 vol/vol) and 10 mL of hydrogen peroxide (30%). The substrate was maintained during 15 min in the cleaning mixture at 70 °C. Finally, it was rinsed with abundant water (Milli Q) and dried under a stream of nitrogen.

2.2. Film preparation

The QD films were prepared by the Langmuir – Blodgett technique (LB) on a Langmuir standard-trough (KSV2000 System 2, Finland) placed in an antivibration table. QD Langmuir monolayers were prepared by deposition of the spreading solution of QDs (10^{-6} M) onto the water subphase with a Hamilton microsyringe with a precision of 1 μL. The subphase temperature was kept constant at (23.0 ± 0.1) °C by flowing thermostated water through jackets at the bottom of the trough. Monolayers were compressed by symmetric barrier compression until they reach a given surface concentration value with the quartz substrate dipped into the trough. The surface density was controlled by the surface pressure value measured with a Pt-Wilhelmy plate connected to an electrobalance. Films were transferred from the air-water interface to the solid by vertically dipping it upward (5 mm min^{-1}) at surface pressure value constant. Surface pressure – area isotherms of both components, CdSe QDs and Gemini surfactant, agree with those previously reported, [26,13]. The methodology and the experimental conditions employed for the bilayer preparation were previously reported [8,14].

Since it is necessary to eliminate spurious variations in the QDs emission quantum yield caused by solvent or dilution effects on the surface conditions of QDs, [21,27–29], we have used only one batch of synthesized QDs. Accordingly, the spreading solutions were prepared in chloroform with the QD powder obtained from a single extraction. The QD solution concentration was kept constant at 10^{-6} M.

2.3. Confocal Fluorescence Lifetime Microscopy (FLIM)

Surface photoluminescence measurements were recorded in a time-resolved fluorescence microscope (MicroTime 200, PicoQuant GmbH). A detailed description was previously reported [30]. In our measurements, the excitation source was a pulsed diode laser emitting at 482 nm with a repetition rate of 2.5 MHz. We used a water immersion objective 60 × magnification with N.A. of 1.2 (UPLSAPO 60XW, Olympus). Samples are scanned with a piezo xy-stage. The emitted fluorescence was cleaned through a dichroic mirror and a bandpass filter with transmission in the interval 550 – 690 nm. To reject out-of-focus light a pinhole of 30 μm was used. The emitted light was detected with single-photon counting avalanche diodes from Perkin-Elmer and digitized using TimeHarp 200 TCSPC PC board (PicoQuant GmbH). The fwhm of instrument response function was around 1 ns and the time increment was 150 ps/channel.

The experimental conditions were the same to those employed in the previous work [8]. Typically, the image scans cover an area of 80×80 μm^2 and are composed of (256×256) pixels. To prevent photo-enhancement effects in QD emission we use an low integration time per pixel, 2 ms [31,32]. The excitation power remained constant at 108 W/cm^2 to minimize multiexcitonic processes. In this condition these processes do not exceed 3.1% of excitation probability [32,33]. The QD luminescence decay is intrinsically complex; therefore, the total number of detected photons per image amounted to a few million counts. On the other hand, the luminescence decays are integrated over the imaged area and can be retrieved from the photon arrival time histogram of all detected photons. The SymPhoTime software (PicoQuant GmbH) was used to analyze the experimental data with a multiexponential function. Fits of decay curves to Eq. (1) was carried out on Matlab software [8]. The quality of the fits was evaluated by the χ^2 parameter and weighted residuals.

2.4. Atomic force microscopy (AFM)

AFM images of the LB films deposited on quartz were obtained in constant repulsive force mode by AFM (Nanotec Dulcinea, Spain) with a rectangular microfabricated silicon nitride cantilever (Olympus OMCL-RC800PSA) with a height of 100 μm, a Si pyramidal tip (radius < 20 nm) and a spring constant of 0.73 N m^{-1}. The scanning frequencies were usually in the range between 0.5 and 2.0 Hz per line. The measurements were carried out under ambient laboratory conditions.

3. Results and discussion

The Langmuir monolayers of different QD surface density were transferred from the air-water interface to a LB film of Gemini surfactant at 30 mN m^{-1}. The surface density was controlled by the surface pressure value. To analyze thoroughly the photoluminescence of QD/Gemini films, multiple fluorescence lifetime images were acquired on each film at different macroscopic positions. From a total of 5 images acquired per sample we have selected representative examples in Fig. 1.

Some dark areas are observed in the image of the lowest QD density (5 mN m^{-1}) and correspond to uncovered regions which are likely due to the low QD concentration. Qualitative information can be extracted from images; thus, when the QD surface concentration is increased, the film coverage increases, however, the image brightness related with the luminescence intensity,

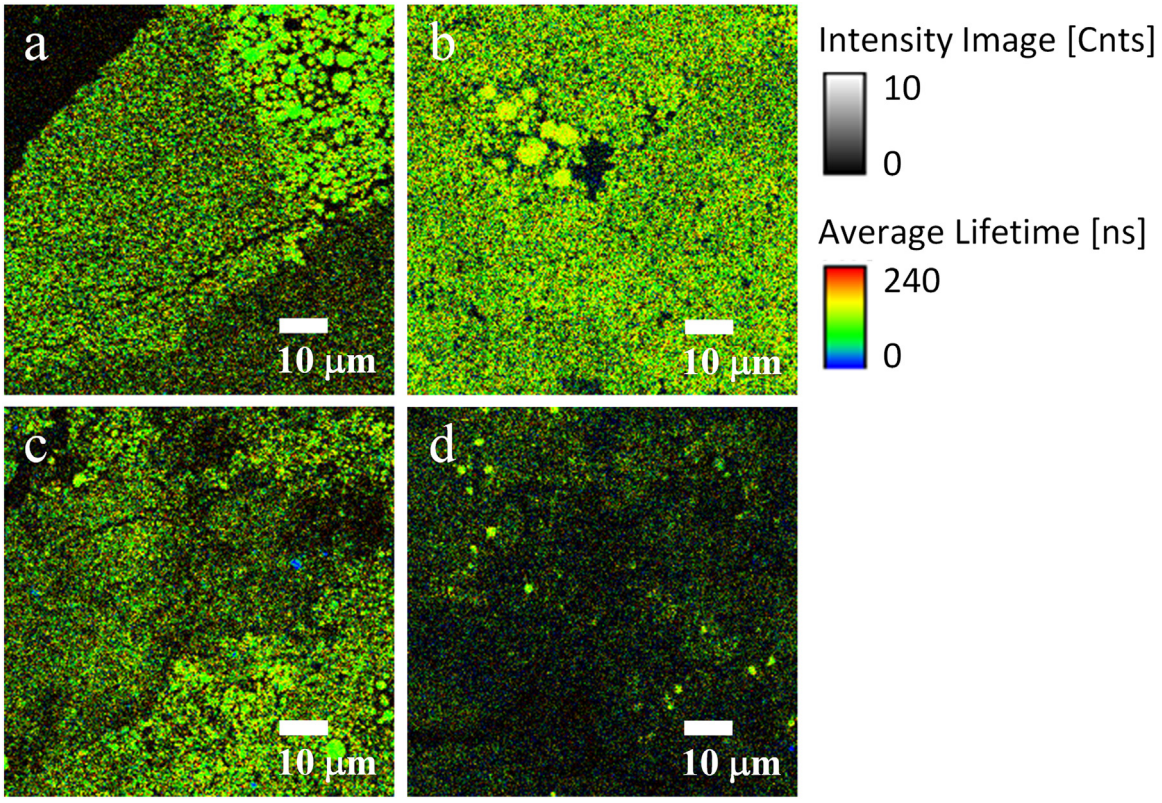

Fig. 1. Representative examples of fluorescence lifetime images for QDs transferred onto a LB film of the Gemini surfactant at 30 mN m^{-1}. The surface pressure values of the QD Langmuir monolayers were: (a) 5 mN m^{-1}; (b) 9 mN m^{-1}; (c) 15 mN m^{-1} and (d) 26 mN m^{-1}.

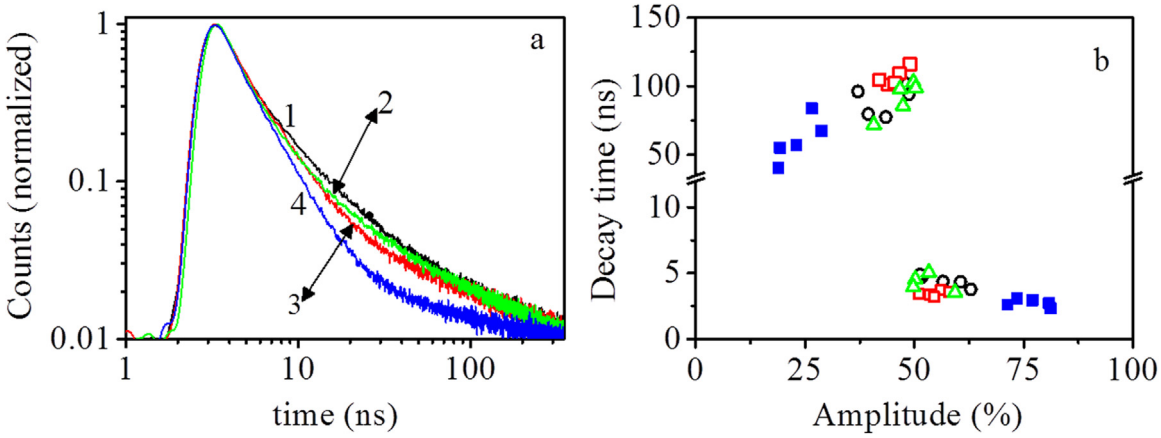

Fig. 2. (a) Photoluminescence decays of QDs deposited onto Gemini surfactant film (30 mN m^{-1}) at the following surface pressure values: curve 1 (5 mN m^{-1}); curve 2 (9 mN m^{-1}); curve 3 (15 mN m^{-1}) and curve 4 (26 mN m^{-1}). (b) Decay times obtained from the multiexponential analysis of each image integrated decay. The decay time of the two faster components are averaged out and are plotted together with the slower decay time. Results correspond to films prepared at the following surface pressure values: open circles (5 mN m^{-1}); triangles (9 mN m^{-1}); open squares (15 mN m^{-1}) and solid squares (26 mN m^{-1}).

drastically decreases for QD films at 26 mN m^{-1}, Fig. 1d. This fact seems to indicate that the magnitude of the nonradiative processes becomes particularly important for the densest films. This behavior is also revealed by fluorescence decay analysis. To illustrate this behavior in Fig. 2a are plotted the photoluminescence decays of films at different QD surface concentration values deposited onto the Gemini film.

The decay curves show that fluorescence decay becomes faster when the QD surface concentration increases. The effect is more noticeable in the decay curve corresponding to 26 mN m^{-1}, curve 4 in Fig. 2a. To quantify this behavior, decays were fitted with a multiexponential function. Three exponential components were required to properly fit the decays. Similar behavior was reported in previous work for mixed films of QDs and the polymer styrene maleic anhydride. In that work, we discussed the complexity of photoluminescence decays of QDs based on our results and on the extensive literature on this subject [8]. Briefly, the core-excited states in CdSe QDs decay with a radiative lifetime of tens of ns. However, the contribution from surface phenomena occurring in organically-capped QDs, such as defect states and charge-trapped states, gives rise to decay components ranging from sub-ns up to hundreds of ns. The fast decay components generally result from the photo-ionization of QDs due to hole trapping in surface defects that accelerates core-exciton recombination [6,34–38]. The long decay components have been attributed to electron injection and trapping in the surrounding media that, at later times, recombines

to a core-excited state giving rise to delayed luminescence [34,35]. Single-particle spectroscopy of CdSe QDs suggests that these emitters display a dynamic heterogeneous behavior, in which the photoluminescence dynamics of an individual particle changes over time [36].

In solid films of QDs, the photoluminescence dynamics are also affected by excitation energy transfer processes due to short interparticle distances between QDs deposited on solids. These processes may contribute to enhance the short decay components because energy migration in the particle lattice increases the probability of excitation energy trapping and quenching. The presence of energy traps in films of QDs has been previously attributed to a minor fraction of QDs with extensive surface defects, or to clusters of QDs strongly packed [39–42]. It has been proved that film morphology plays a crucial role; thus, regular rearrangements of QDs on the solid avoid the formation of clusters which quench the QDs photoluminescence by excitation energy trapping [8].

As was evidenced in the previous work, a simplified way of analyzing the multiexponential decays is to compare the amplitude of short and long decay times of different films by plotting the short decay times averaged out using the respective intensity-weight values together with the long decay times against the amplitude [8], Fig. 2b. This choice of representation allows us to compare separately the long decay component due to delayed luminescence with the short components more strongly influenced by energy migration and film morphology.

Results in the Fig. 2b show that the decay times of QDs films at low surface pressure are quite similar; however, for those corresponding to the densest film, 26 mN m^{-1}, the fastest component prevails. All experimental information shows that the contribution of nonradiative processes increases with the QDs surface density.

For comparative purposes we have measured the photoluminescence decays of QD films directly deposited onto the quartz substrate. The experimental conditions were the same employed for films of QDs deposited on the Gemini surfactant film. Fig. 3 shows representative images of QDs films at the surface pressure values of 5, 9 and 26 mN m^{-1}, respectively.

The FLIM images clearly revealed regions constituted by circular aggregates together with regions in which non-aggregated QDs predominate. Insets on Figs. 3a and b are magnifications to show the morphology of aggregates. 3D aggregation of QDs directly deposited onto the substrate was previously reported and has been attributed to the weak interactions between the hydrophobic chains of the QD capping agent (TOPO) and the solid substrate. AFM results demonstrated that the aggregate height increases with the QDs surface density and the height values are consistent with 3D aggregates constituted by 2–5 QDs [13,14].

The decay curves of different regions of QDs supported onto quartz were analyzed and results showed that the fluorescence decays are faster in the regions of 3D aggregates than in the non-aggregates ones. This behavior is illustrated in Fig. 4 that shows FLIM images of QDs deposited directly on quartz at surface pressure values of 5 and 9 mN m^{-1}, and below, the decay curves extracted from the regions marked in the FLIM images.

The decays shown in Figs. 4d and e are taken from regions without (blue curves) and with aggregation of QDs (red curves), respectively. At a given surface pressure, the decays for regions with QDs aggregation are faster than those for regions without aggregation. However, the decay tails at long time show a similar slope for these two situations (red and blue curves). Therefore, the main difference between decays resides in the contribution of the short decay components, which is larger for the regions with QDs aggregation. As referred to above, the photoluminescence dynamics in solid films of QDs are affected at short decay times by excitation energy trapping processes. The larger contribution of the short decay components in our systems could be attributed to an increased contribution from energy migration and trapping processes due to the larger density of particles within QD aggregates. Interestingly, the decays also become faster upon increasing surface pressure from 5 to 26 mN m^{-1}, which is in qualitative agreement with the role attributed to particle density in the photoluminescence of QD films.

Fig. 5a shows the FLIM image of QDs deposited on the Gemini surfactant film. The photoluminescence decays plotted in Fig. 5b correspond to regions marked as 9 and 10 in Fig. 5a. For the sake of comparison, decays of QD films directly deposited onto quartz and marked as regions 6 and 7 in Figs. 4b and c of QD are also plotted in Fig. 5b. As can be seen in Fig. 5b, decays present similar slope of the decay tail at long times while the main differences are observed in the relative contributions of short decay components.

Although visual inspection of the decays allows us to infer qualitative information about the relative contribution of short vs. long decay components, that is not enough to evaluate the influence of short components in aggregated and non-aggregated regions. For this purpose, we have fitted the decays with a phenomenological model previously reported by us, which gave evidence of the important role of the film morphology on the photoluminescence properties of QDs films [8]. The model considers the decay function as a sum of two separate contributions, Eq. (1).

$$D(t) = \sigma\, S(t) + (1-\sigma)\, C(t) \quad (1)$$

The first contribution, S(t), describes the luminescence decays affected by recombination from charge trapped to core excited states according to the Tachiya-Mozumber model [43,44]. This model considers a mechanism of charge trapping by electron tunneling toward a uniform distribution of traps and in our case is defined by:

$$S(t) \approx \exp\left[-t\, k_r/(1 + k_{ct}\, \tau_0)\right] \quad (2)$$

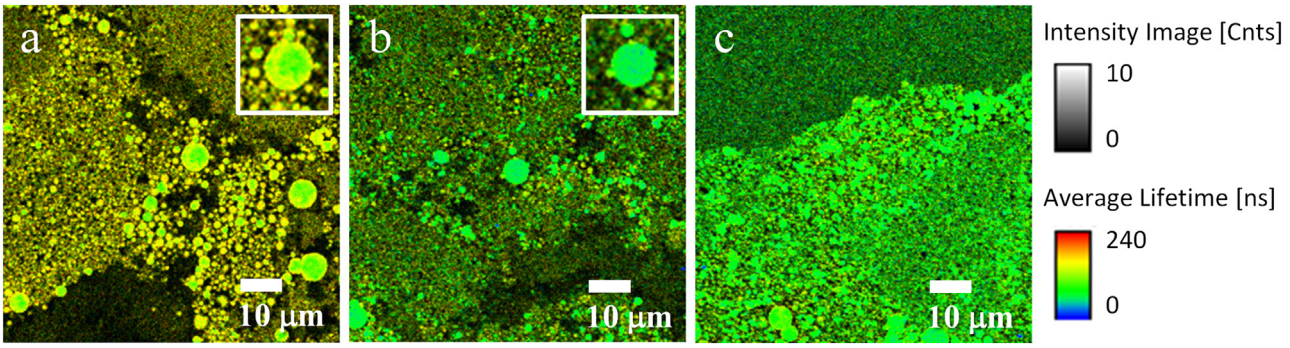

Fig. 3. Fluorescence Lifetime Images of QDs deposited onto quartz at the surface pressure values of: 5 (a), 9 (b) and 26 (c) mN m^{-1}. Insets in (a) and (b) are magnifications of spherical aggregates in figures.

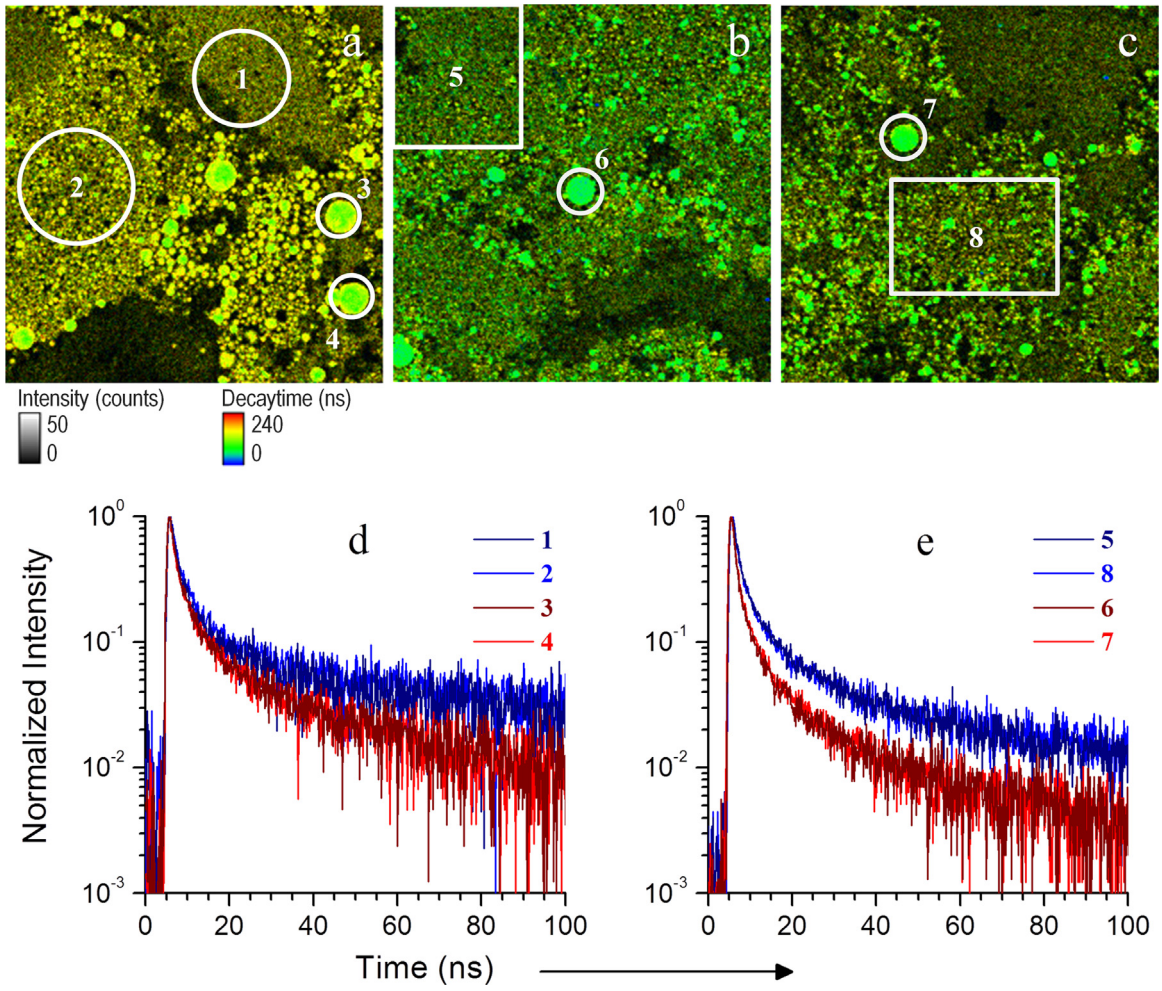

Fig. 4. (a–c) FLIM images of QDs films deposited onto quartz at the surface pressure value of 5 mN m^{-1} (a) and 9 mN m^{-1} (b and c). The numbered circles and squares show the regions of interest selected to extract photoluminescence decays from these images. (d and e) Photoluminescence decays of regions marked as numbers 1–8 in Fig. 4a–c. The blue and red curves illustrate decay curves from regions of films without and with aggregation of QDs, respectively. (For interpretation of the references to color in this figure legend, the reader is referred to the web version of this article.).

In Eq. (2), k_r represents the radiative recombination rate and $\tau_0^{\mu} k_{ct}$ the charge transfer rate term. These parameters represent intrinsic photophysical properties of the CdSe QD [45].

The second contribution, C(t), is related with the energy transport according to the model developed by Fayer [46,47]. This model was proposed to interpret the excitation transfer in disordered two-dimensional systems with randomly distributed donor and trap species. The two-dimensional approach is used here in first approximation for the 3D aggregated film regions, in view of their shallow thickness of only 2–5 QDs, as referred to above. In the model, the transport master equation uses the diagrammatic expansion of the Green's function to obtain the probability $P_D(t)$ of finding an excitation at a given position r at time t.[8] The corresponding decay law is obtained multiplying $P_D(t)$ by a decaying exponential with the donor lifetime:

$$C(t) = \exp\left[-t/\tau_D\right] x \; P_D(t) \tag{3}$$

The fitting with Eq. (1) of the decays of QD films deposited directly on the substrate and on the Gemini surfactant Langmuir-Blodgett film are shown in Figs. S1 and S2 of the Supporting Material and the parameters obtained in fits are collected in Tables 1 and 2, respectively. Results in Table 1 correspond to decays of regions without 3D aggregation while the data in Table 2 correspond to decays of 3D aggregates. The values of parameters $\tau_0^{\mu} k_{ct}$ and $1+\mu$ retrieved from the fits were found to be rather similar to their initial guesses, which by its turn were chosen according to our previous results [8]. For this reason, these parameters were kept constant at $\tau_0^{\mu} k_{ct}=2$ and $1+\mu=1.95$ in the fits that yielded the values given in Tables 1 and 2. The same approach could be applied to the radiative lifetime value, which does not vary much from the initial guess of $k_r^{-1}=30$ ns. This set of model parameters describes intrinsic properties of the QDs used, or of their immediate surroundings, such as the organic coating layer. Therefore, it is reasonable to assume that these parameters are constant throughout the fits, leaving as adjustable only those parameters which depend on the film morphology, such as the number density of donors and traps, C_D, C_T and the relative contribution to the decay σ.

From data in Tables 1 and 2, it is possible to conclude that the number density of donors, C_D, obtained from the fit process is almost the same for the different zones and the value found for these systems is also the same to that calculated for QDs/ PS-MA-BEE films [8]. Conversely, both, the number density of traps, C_T, and, σ, seem to be different for the distinct films.

According to the qualitative interpretation of decays presented above, the main differences between decays are observed at short times. Therefore, since the photoluminescence dynamics in QD films are affected at short decay times by excitation energy trapping processes, we analyze the variation of relative contribution to

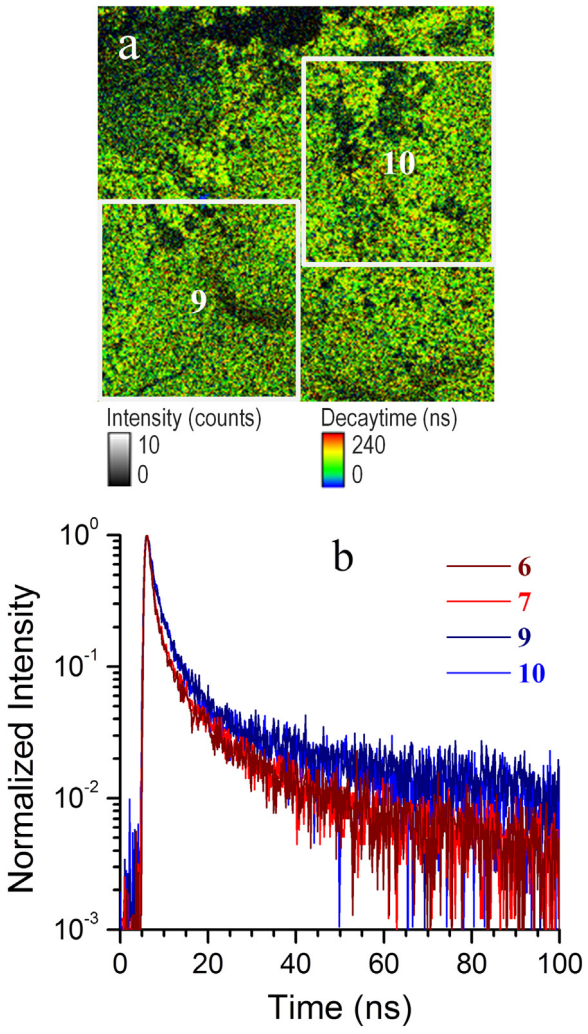

Fig. 5. (a) FLIM image of QDs films deposited onto Gemini surfactant film at the surface pressure value of 9 mN m^{-1}. The numbered squares show the regions of interest selected to extract photoluminescence decays from this image. (b) Photoluminescence decays of regions marked as numbers 6 and 7 in Figs. 4b and 4c (red curves), and as number 9 and 10 in Fig. 5a (blue curves). (For interpretation of the references to color in this figure legend, the reader is referred to the web version of this article.).

Table 1
Parameters Fitted with Eq. (1) to Photoluminescence Decays of CdSe QDs in regions without 3D aggregates.

Region analyzed π (mN/m)	A7 5 mN/m	C3 5 mN/m	C6 5 mN/m	A8 9 mN/m	A9 9 mN/m	A15 9 mN/m
k_r^{-1}(ns)	29.84	30.19	29.96	29.80	29.81	30.01
σ	0.278	0.264	0.245	0.119	0.138	0.253
C_D	3.12	3.35	3.04	3.10	3.26	3.32
C_T	0.375	0.386	0.435	0.621	0.666	0.424
χ^2	1.067	1.122	1.086	1.235	1.084	1.199

decays of the energy transfer process, 1-σ, with the surface density and trap concentration, respectively. With this purpose, in Fig. 6a the relative contribution of energy transport component to the decay, 1-σ, is plotted against the surface density, controlled by surface the pressure value, π. The 1-σ values plotted in Fig. 6a are averaged for each surface pressure value and the error bars correspond to the standard deviation.

As can be seen in Fig. 6a the relative contribution to the decay of energy transport processes increases when the surface pressure increases. Moreover, the contribution values are higher for films

Table 2
Parameters Fitted with Eq. (1) to Photoluminescence Decays of CdSe QD 3D aggregates.

Region analyzed π (mN/m)	C1 5 mN/m	C2 5 mN/m	C10 9 mN/m	C11 9 mN/m	C12 26 mN/m	C13 26 mN/m
k_r^{-1} (ns)	30.23	30.27	29.92	29.93	29.78	29.81
σ	0.236	0.225	0.099	0.130	0.201	0.040
C_D	3.27	3.28	3.34	3.25	3.37	3.58
C_T	0.350	0.331	0.27	0.331	0.358	0.173
χ^2	1.192	1.253	1.791	1.478	1.184	1.930

with 3D aggregates than for QD films without aggregation. This behavior is expected if one considers that energy transport processes are related with short interparticle distance and the distance between QDs decreases when films are strongly packed. Thus, the interparticle distance decreases as the surface density increases and consequently, the relative contribution of energy transport is larger for dense films, high surface pressure values, and for films with 3D aggregates which contain a great number of particles for each circular aggregate.

Results also revealed an increase of the relative contribution to the decay of the energy transport with trap concentration, Fig. 6b, for QDs films without 3D aggregation. As can be seen in Table 1 and Fig. 6b, in non-aggregated films the trap concentration increases as the QD surface concentration. This behavior seems to be consistent with the fact that the energy traps can be attributed to clusters of QDs highly packed [8] and consequently, increase as surface density increases. The replacement of the stabilizer, TOPO, by the Gemini surfactant could be responsible of this behavior. However, the partial replacement of TOPO by molecules containing carboxylic or thiol groups which can interact with the surface core Cd^{2+} is carried out in solution and under sonication or reflux conditions [48]. Since all these conditions are not fulfilled in our system this contribution should not be considered. On the other hand, the relative contribution to the decay of the energy transport process is higher for films with 3D aggregates than for QDs without aggregation, although the trap concentration calculated from fits seems to be lower for films with 3D aggregates than for the non-aggregated ones. Besides, the contribution of the energy transport process in 3D aggregates films increases with the QD surface density. It should be noticed that in films with 3D aggregates, the aggregate height increases with the QD surface density, [13,14] accordingly, the number of QD particles closely packed in 3D aggregates also increases with surface density. Therefore, it is possible to suggest that the number of QDs with short interparticle distance which favors the energy transfer processes increases for films with 3D aggregates, while the density of energy traps of QDs in the 3D aggregates seems to be on average lower than in films without QD aggregation. Other contributions, such as degradation by oxidation [49] and the influence of free capping ligands entrapped on the aggregates could be considered as responsible of this behavior. However, because free capping ligands were removed along other molecules of the reaction medium in the purification processes, this contribution does not seem the main contribution for the observed behavior. In addition, as no significant changes between the photoluminescence decays of films stored in vacuum desiccators over several months were observed, we think that the decrease of interparticle distance in films with 3D aggregates can be the main contribution of the increased energy transfer observed, although more efforts must be done in the future to interpret this behavior.

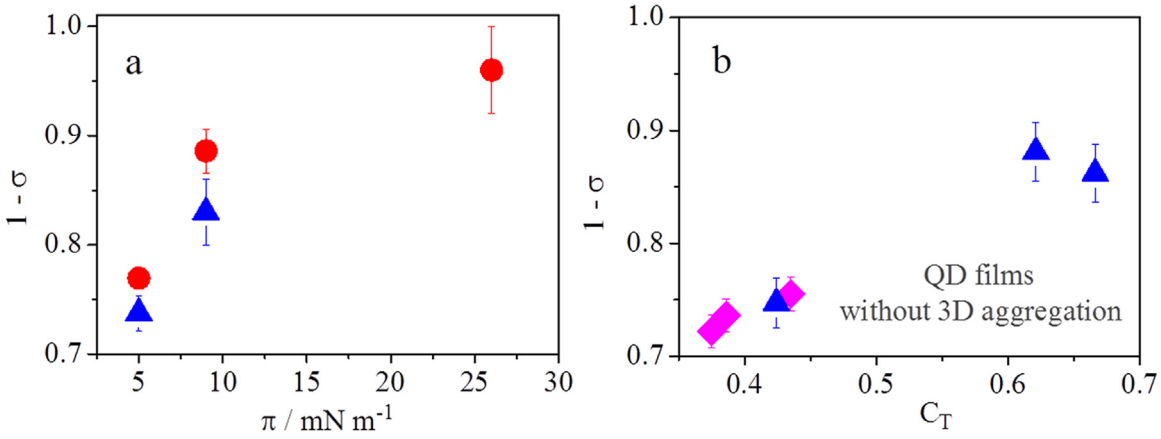

Fig. 6. Variation of the relative contribution to the decay of the energy transport component, 1-σ, with: (a) the surface density of QDs measured as surface pressure, π; and (b) concentrations of traps. Symbols in Fig. 6a represent: circles (regions of 3D aggregates) and triangles (regions without aggregation). Symbols in Fig. 6b correspond to: diamonds, films transferred at 5 mN m^{-1} and triangles at 9 mN m^{-1}.

4. Conclusions

The effect of 3D aggregates on the photoluminescence of QD films was studied by analyzing the photoluminescence dynamics of QD films directly deposited onto quartz and deposited onto a Langmuir-Blodgett film of a Gemini surfactant. The surfactant film avoids the QD aggregation [14] and thus films with regions of QD 3D aggregates were observed in films of QDs directly deposited onto quartz. The photoluminescence decays were interpreted according to a phenomenological model previously reported by us [8]. The model considers that QD photoluminescence is affected by energy transport and trapping processes and the efficiency of these processes depends essentially on the energy traps. Our results demonstrated that the trap concentration increases with the surface concentration. We have also proved that in films without 3D aggregation the relative contribution to decay of the energy transport process increases as the trap concentration increases. Finally, our results show that in films with 3D aggregates, the contribution of the energy transfer process is higher than that corresponding to QD films without 3D aggregates. This fact could be attributed to the decrease of interparticle distance in films with 3D aggregates.

Acknowledgments

The authors thank financial support from ERDF and MEC (grant number MAT 2010-19727). T. Alejo wishes to thank the European Social Fund and Consejería de Educación de la Junta de Castilla y León for her FPI grants. P.M.R.P. acknowledges Program Ciência 2008 from FCT. Thanks are due to Fundação para a Ciência e a Tecnologia (FCT, Portugal) for 3° Quadro Comunitário de Apoio (FEDER); FCT/Re-equipment Project 115/QUI/2005.

Appendix A. Supplementary material

Supplementary data associated with this article can be found in the online version at http://dx.doi.org/10.1016/j.jlumin.2016.11.002.

References

[1] S. Coe, W.-K. Woo, M. Bawendi, V. Bulovic, Nature 420 (6917) (2002) 800.
[2] A.L. Efros, M. Rosen, M. Kuno, M. Nirmal, D.J. Norris, M. Bawendi, Phys. Rev. B 54 (7) (1996) 4843.
[3] C. Wang, B.L. Wehrenberg, C.Y. Woo, P. Guyot-Sionnest, J. Phys. Chem. B 108/26 108 (26) (2004) 9027.
[4] J. Wang, D. Vennerberg, Z. Lin, J. Nanoeng. Nanomanuf. 1 (2) (2011) 155.
[5] L.E. Brus, J. Chem. Phys. 80 (9) (1984) 4403.
[6] M.G. Bawendi, P.J. Carroll, W.L. Wilson, L.E. Brus, J. Chem. Phys. 96 (2) (1992) 946.
[7] Cd.M. Donega, Chem. Soc. Rev. 40 (3) (2011) 1512.
[8] B. Martín-García, P.M.R. Paulo, S.M.B. Costa, M.M. Velázquez, J. Phys. Chem. C 117 (28) (2013) 14787.
[9] G. Zhavnerko, G. Marletta, Mater. Sci. Eng. B 169 (1–3) (2010) 43.
[10] Y.-J. Shen, Y.-L. Lee, Y.-M. Yang, J. Phys. Chem. B 110 (19) (2006) 9556.
[11] M.M. Velázquez, T. Alejo, D. López-Díaz, B. Martín-García, M.D. Merchán, in: P. K. Nayak (Ed.), Two-dimensional Materials: Synthesis, Characterization and Potential Applications, (Chap. 2), 2016, pp. 21–42.
[12] T. Alejo, M.D. Merchán, M.M. Velázquez, Thin Solid Films 519 (16) (2011) 5689.
[13] T. Alejo, M.D. Merchán, M.M. Velázquez, J.A. Pérez-Hernández, Mat. Chem. Phys. 138 (1) (2013) 286.
[14] T. Alejo, B. Martín-García, M.D. Merchán, M.M. Velázquez, J. Nanomater. (2013) 1.
[15] B. Martín-García, M.M. Velázquez, Mater. Chem. Phys. 141 (1) (2013) 324.
[16] B. Martín-García, M.M. Velázquez, Langmuir 30 (2) (2014) 9977–9984.
[17] W.W. Yu, X. Peng, Angew. Chem. Int. Ed. Engl. 41 (13) (2002) 2368.
[18] N. Tomczak, D. Jaczewski, M. Han, G.J. Vancso, Prog. Polym. Sci. 34 (5) (2009) 393.
[19] J. Jasieniak, L. Smith, Jv Embden, P. Mulvaney, M. Califano, J. Phys. Chem. C 113 (45) (2009) 19468.
[20] J.T. Kopping, T.E. Patten, J. Am. Chem. Soc. 130 (2008) 5689..
[21] J.S. Owen, J. Park, P.E. Trudeau, A.P. Alivisatos, J. Am. Chem. Soc. 130 (2008) 12279.
[22] A.J. Morris-Cohen, M.D. Donakowski, K.E. Knowles, E.A. Weiss, J. Phys. Chem. C 114 (2) (2009) 897.
[23] R. Zana, M. Benrraou, R. Rueff, Langmuir 7 (6) (1991) 1072.
[24] W. Kern, J. Electrochem. Soc. 137 (6) (1990) 1887.
[25] W. Kem, Handbook of Semiconductor Wafer Cleaning Technology, Noyes Publications, New Jersey, 1993.
[26] K.M. Gattas-Asfura, C.A. Constantine, M.J. Lynn, D.A. Thimann, X. Ji, R. M. Leblanc, J. Am. Chem. Soc. 127 (42) (2005) 14640.
[27] G. Kalyuzhny, R.W. Murray, J. Phys. Chem. B 109 (15) (2005) 7012.
[28] C. Bullen, P. Mulvaney, Langmuir 22 (2006) 3007.
[29] A.M. Munro, I. Jen-La Plante, M.S. Ng, D.S. Ginger, J. Phys. Chem. C 111 (17) (2007) 6220.
[30] P.M.R. Paulo, S.M.B. Costa, J. Phys. Chem. C 114 (44) (2010) 19035.
[31] M. Simurda, P. Nemec, F. Trojánek, P. Malý, Thin Solid Films 453–454 (0) (2004) 300.
[32] K. Pechstedt, T. Whittle, J. Baumberg, T. Melvin, J. Phys. Chem. C 114 (28) (2010) 12069.
[33] N. Ganesh, Zhang, W. Mathias, P.C. Chow, E. Soares, J.A.N.T. Malyarchuk, V. Smith, A.D. Cunningham, B.T, Nat. Nanotechnol. 2 (2007) 515.
[34] M. Jones, S.S. Lo, G.D. Scholes, J. Phys. Chem. C 113 (42) (2009) 18632.
[35] P.H. Sher, J.M. Smith, P.A. Dalgarno, R.J. Warburton, X. Chen, P.J. Dobson, S. M. Daniels, N.L. Pickett, P. O'Brien, Appl. Phys. Lett. 92 (10) (2008) 101111.
[36] B.R. Fisher, H.-J. Eisler, N.E. Stott, M.G. Bawendi, J. Phys. Chem. B 108 (1) (2004) 143.
[37] L. Hartmann, A. Kumar, M. Welker, A. Fiore, C. Julien-Rabant, M. Gromova, M. Bardet, P. Reiss, P.N.W. Baxter, F. Chandezon, R.B. Pansu, ACS Nano 6 (10) (2012) 9033.
[38] J.L. Nadeau, L. Carlini, D. Suffern, O. Ivanova, S.E. Bradforth, J. Phys. Chem. C 116 (4) (2012) 2728.
[39] D.P. Shepherd, K.J. Whitcomb, K.K. Milligan, P.M. Goodwin, M.P. Gelfand, A.

Van Orden, J. Phys. Chem. C 114 (35) (2010) 14831.
[40] R. Koole, P. Liljeroth, C. de Mello Donegá, D. Vanmaekelbergh, A. Meijerink, J. Am. Chem. Soc. 128 (32) (2006) 10436.
[41] J.D. Lee, S. Maenosono, Phys. Rev. B 80 (20) (2009) 205327.
[42] M. Yu, A. Van Orden, Phys. Rev. Lett. 97 (23) (2006) 237402.
[43] M. Tachiya, A. Mozumder, Chem. Phys. Lett. 34 (1) (1975) 77.
[44] M. Tachiya, K. Seki, Appl. Phys. Lett. 94/8 (2009) 081104.
[45] A.L. Rogach, Semiconductor Nanocrystal Quantum Dots: Synthesis, Assembly, Spectroscopy and Applications, Springer:Wien, New York, 2008.
[46] C.R. Gochanour, H.C. Andersen, M.D. Fayer, J. Chem. Phys. 70 (9) (1979) 4254.
[47] R.F. Loring, M.D. Fayer, Chem. Phys. 70 (1–2) (1982) 139.
[48] N. Tomczak, D. Janczweski, M. Han, G.J. Vancso, Prog. Polym. Sci. 34 (2009) 393.
[49] R. Quintero-Torres, C.A. Foell, J. Pichaandi, F.C.J.M. van Veggel, J.F. Young, Appl. Phys. Lett. 101 (12) (2012) 121904.